Data analysis procedure

S. Bourdarie (ONERA - France)
B. Blake (Aerospace Corporation – USA)
J.B. Cao (CSSAR – China)
R. Friedel (LANL – USA)
Y. Miyoshi (STELAB – Japan)
M. Panasyuk (MSU – Russia)
C. Underwood (U. Of Surrey – UK)

I. Introduction

The purpose of this document is to delineate analysis methodologies for creating improved space radiation models from a wide variety of space radiation measurements collected worldwide.

The energetic particle environment near the Earth is composed of three different components:

1. The radiation belts where energetic electrons and ions can be found. This ionizing environment can be highly dynamic during magnetic storms,

2. The solar energetic particles (mainly protons and heavy ions), which are present only during Solar Particle Events, with a duration of hours to days,

3. The Galactic cosmic rays (mainly protons and heavy ions)

Of course all these particles cohabit in space and their measurement is not at all straightforward. The consequence is that all measurements have to be analyzed in detail based upon our current knowledge of radiation belt global structure and dynamics as well as instrument physics. This analysis has to focus on instrument contamination, saturation, background, glitches … and cross-calibration.

Guidance is needed from the worldwide community of developers of space radiation models to permit standardization of data analysis efforts to ensure that everybody is working on the same basis and to increase our confidence in the quality of the data actually used in models.

Note that in the following document we suppose that the instrument response (based on Monte-Carlo simulation and/or ground tests) is known well enough to make good use of the data, in particular this means that the counts to flux conversions are known.

In this documents examples of problems encountered with several instruments are shown. Various spacecraft/instruments, from different countries, built with different technologies have been chosen to show that the perfect instrument does not exist, and that most instruments have advantages and deficiencies for space modeling. In any case there is no desire to one point fingers at "bad" or "good" instruments but to show that with the proper analysis useful data can be derived from almost any of these instruments.

II. Context

Nowadays there are large data bases of radiation-belt and interplanetary-medium energetic particles available throughout the world. Of course in future years more such data bases will become available. What currently exists already is a very useful and important resource that can be effectively used to develop new space environment models. These data have been recorded by a wide variety of instruments, which have varied characteristics. It is obvious that these characteristics have to be understood for future use of these in-situ data for modeling. Data from different sources have to be merged together and well understood to ensure a global coherence.

A fundamental requirement for our modeling purposes is the availability of multi-instrument, multi-spacecraft data that are inter-calibrated. Here the term "inter-calibrated" means that the response functions of all instruments must be well known so that these data can be seamlessly merged. Ideally, given "perfect" instruments, no further efforts along these lines would be required. However energetic particles represent a challenging measurement task in space for many reasons. One critical reason is it is never possible to fly the amount of shielding required for a "clean" measurement, and a second is that it is impossible to recreate the full energetic particle environment the instrument will encounter in space in the lab for calibrations. Existing instrument calibrations range from comprehensive to virtually non-

existent. Some laboratory calibrations are mainly limited to "through the aperture" calibrations which do not address the instruments background response to an omnidirectional, highenergy environment. For some instruments flown on a series of satellites (e.g. LANL-GPS, LANL-GEO) detailed calibrations were only performed for one representative instrument of many "identical" instruments. In the case of other instruments, only the "nominal" design specifications are available to the radiation-belt modeler. Designs of instruments vary widely, with some intrinsically having better immunity to background than others.

While there has been much progress in the modeling of energetic particle instruments from first principles, those methods have their own challenges and still often give factors of 2-5 uncertainties in an instrument's performance [Cayton and Tuszewski, 2005]. Full modeling of space radiation instruments is a time and computer-intensive procedure, and has only been done for a few instruments (e.g. LANL-GPS, some LANL-GEO). These instrument-modeling studies can also tell under what conditions an instrument will perform well, and when it might be in principle impossible to recover a "clean" spectrum from an instrument.

Given the limitations of each individual instrument's pre-flight calibrations, further, on-orbit, inter-comparisons using actual, collected data need to be performed.

III. Coordinates to sort the data

A first step to go through before analyzing on-orbit measurements is to define appropriate coordinates to sort the data. The basic positional information associated with any in-situ measurements is the time and location in geographic coordinates. Because the trapped particle motion is governed by the Earth's magnetic field (see annex A), magnetic coordinates have to be computed to organize the data..

III.1 Set of coordinates

Because the Earth magnetic field is not constant in time the best set of parameters to use are the three adiabatic invariants J_1, J_2 and J_3 (see annex A). Unfortunately this coordinate system has some limitations: it is only appropriate for trapped particles and not for cold plasma data, measurements are always done at constant energy (this means different J_1 and J_2 for each measurements) and from the physics point of view it is easier to manipulate variables like energy and pitch angle.

Because in a slowly varying magnetic field only K (J_1-J_2) and L* (J_3) are conserved along a trapped particle motion, a good consensus is to adopt the following set of coordinates: **E,** α_{eq}^***, L*,** and **MLT,**

where E is the particle energy, α_{eq}^* is deduced from the equation $\dfrac{K\sqrt{L*}}{Re\sqrt{Bo}} = \dfrac{Y(y)}{y}$

($y = \sin(\alpha_{eq}^*)$ and Y(y)= 2.760346 + 2.357194y − 5.117540y$^{3/4}$), L* is the Roederer L parameter and MLT the magnetic local time (crucial for non-trapped particles).

This set of parameters has two advantages; they may easily be computed from measurements, and they are convenient to use for performing data assimilation in physical radiation belt models.

III.2 Magnetic field model

An ideal magnetic field model is one which allows removal of adiabatic flux variations when data are sorted according to J_1, J_2 and J_3. Unfortunately, though there are many time dependant magnetic field models available, none of them are realistic enough during very disturbed periods to sort the data properly (one magnetic field model can be better at low L*, another one better on the day side, etc …). Moreover for sophisticated, external magnetic field models various input are required. For the simplest, magnetic indices are sufficient but for some others solar-wind parameters are necessary. Both can be used. Nevertheless, if in-situ radiation-belt particle data are analyzed in order to develop a radiation-belt model, measurements from long duration satellites must be considered and solar wind parameters may not always be available. Moreover, computing L* with such models over decades of measurements would be very computer intensive. Thus for this purpose it is preferable to select a model which is not dependent upon solar wind parameters. Only a few choices are left: Mead-Fairfield 1975, Tsyganenko 1987 and 1989 and Olson Pfitzer quiet 1977. From statistical studies the Olson-Pfitzer quiet model has been shown to be a good average external magnetic field model when compared to measurements.

For the internal magnetic field, the use of the IGRF reference field is well established. Because this field is slowly drifting in time (secular drift) updating IGRF once per year is usually sufficient and it can be done at each mid-year.

Therefore the proposed standard for the magnetic field model is IGRF (decimal year + 0.5) plus Olson-Pfitzer quiet 1977.

IV Obtaining sanitized data

In the following sections the terms contamination and background are defined such as:
"contamination" = high level dynamic background due to non primary instrument response that can completely dominate an instruments response
"background" = low level more or less constant background due to electronic and detector noise and cosmic rays.

IV.1 Electron data contamination

IV.1.1 Contamination by proton

It is well known that during times of solar energetic proton events (SEPs) many of the detectors are contaminated with strong background counts. Figure 1 gives an example of a period of SEP contamination. The SEP event is clearly visible in the elevated flux levels of energetic protons measured at GOES 08. These ions can penetrate the electron detectors at

LANL-GPS and LANL-GEO, leading to elevated electron flux observations, across all sampled L-values, as clearly shown in Figure 1.
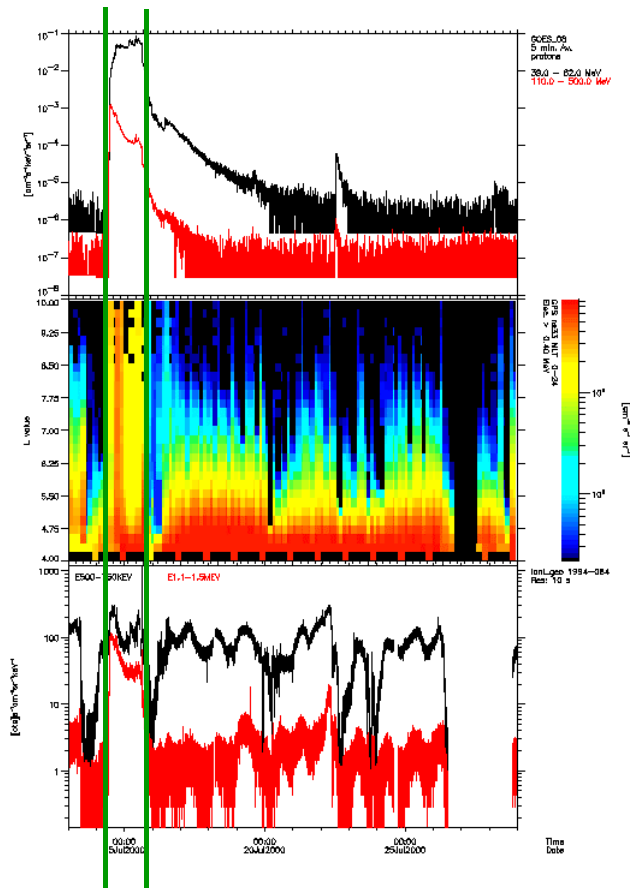

Figure 1 : Example of SEP data from GOES 8 [top panel] leading to contamination in data from the LANL-GPS [middle panel] and LANL-GEO [bottom panel] instruments. The SEP period is between the two vertical green lines.

[Ed. Note: there are degrees of contamination. Even if electrons dominate, the data can be compromised.] Next, depending on the instrument there may be regions in the orbit where we know that the data is contaminated by background. This can be easily seen from survey plots where fluxes are color coded in a L* versus time map. Such an example is provided in Figure 2. In the bottom panel (the 1.24-1.6 MeV channel) contamination induced by SEPs in the outer belt (brief enhancements across L* > 4) and contamination induced by trapped protons in the south Atlantic anomaly (L*<2.5) is clearly seen. It must be noted here that in this case, if data are contaminated by SEPs (which is more obvious to detect) there is high probability that the same channel is contaminated by high-energy trapped protons in the inner belt. In the lower electron channel (top panel), because electron fluxes probably dominate high-energy proton fluxes which could induce background, contamination is masked and electrons dominate in that channel.
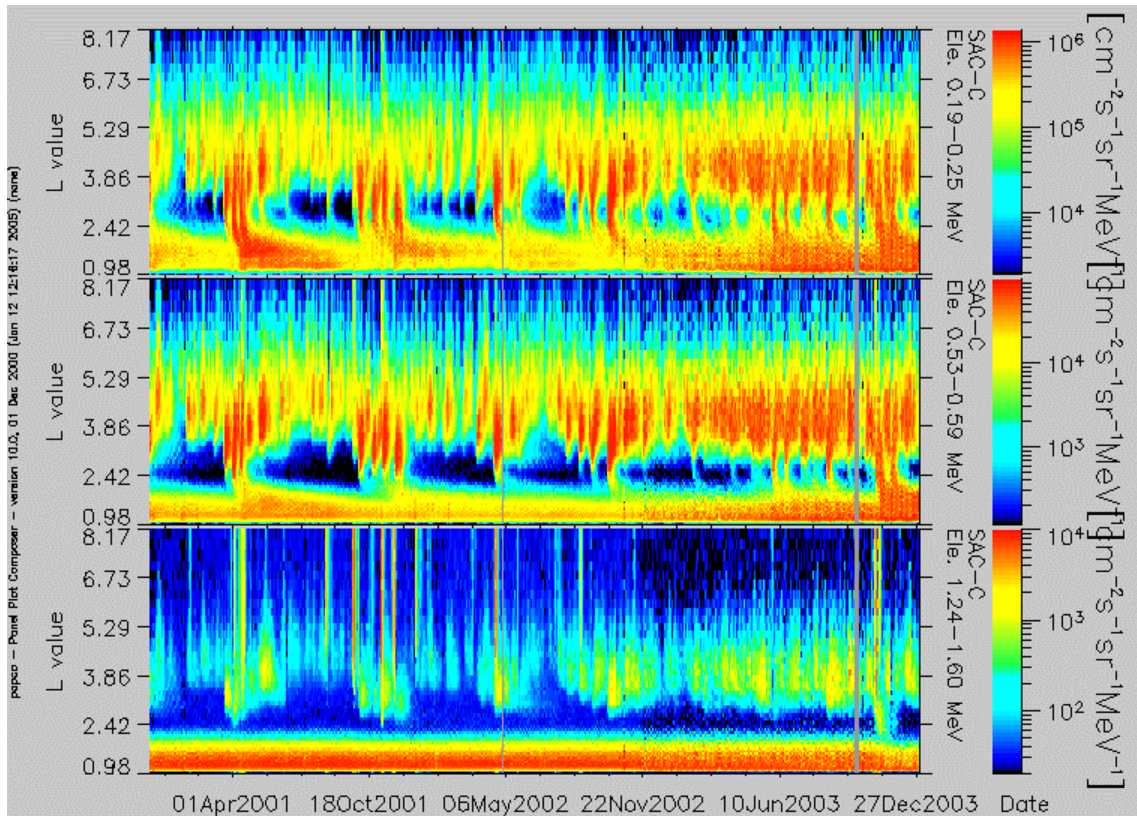
Figure 2 : Electron flux on-board SAC-C spacecraft (715 km – 98°) in a L* versus time map for three energies (top=0.19-0.25 MeV, middle=0.53-0.69 MeV and bottom=1.24-1.6 MeV)

To clean up the data two possibilities emerge. For the first one let's consider the case there are no proton measurements (or at least not in the energy range responsible for any background) on the same spacecraft. In this case, the analysis must be done in two steps:

1- To evaluate any possible contamination due to SEPs GOES proton data can be used as a proxy. It is then necessary to plot electron data (at the same resolution as GOES) when the spacecraft in question is outside of geomagnetic shielding, L*>7 is a safe value, but it must be lower for GEO orbit) versus GOES data for each time step. In this case it is necessary to find out the best correlation obtained by using various GOES proton channels. Such an example is given in Figure 3 where LANL-GEO-ESP electron (4.5-6. MeV) is plotted versus GOES-08 15-44 MeV proton. When GOES measurements (on the x axis) is greater than the value indicated by the vertical green line, then SEP protons are recorded on-board GOES. On the right hand side of the plot a clear correlation is seen between LANL and GOES data. Finally all LANL data (for this energy channel) below the red line must be removed, as they correspond to contamination. The equation of the red line indicates the boundary where LANL data must be removed using GOES-08 measurements as a proxy.
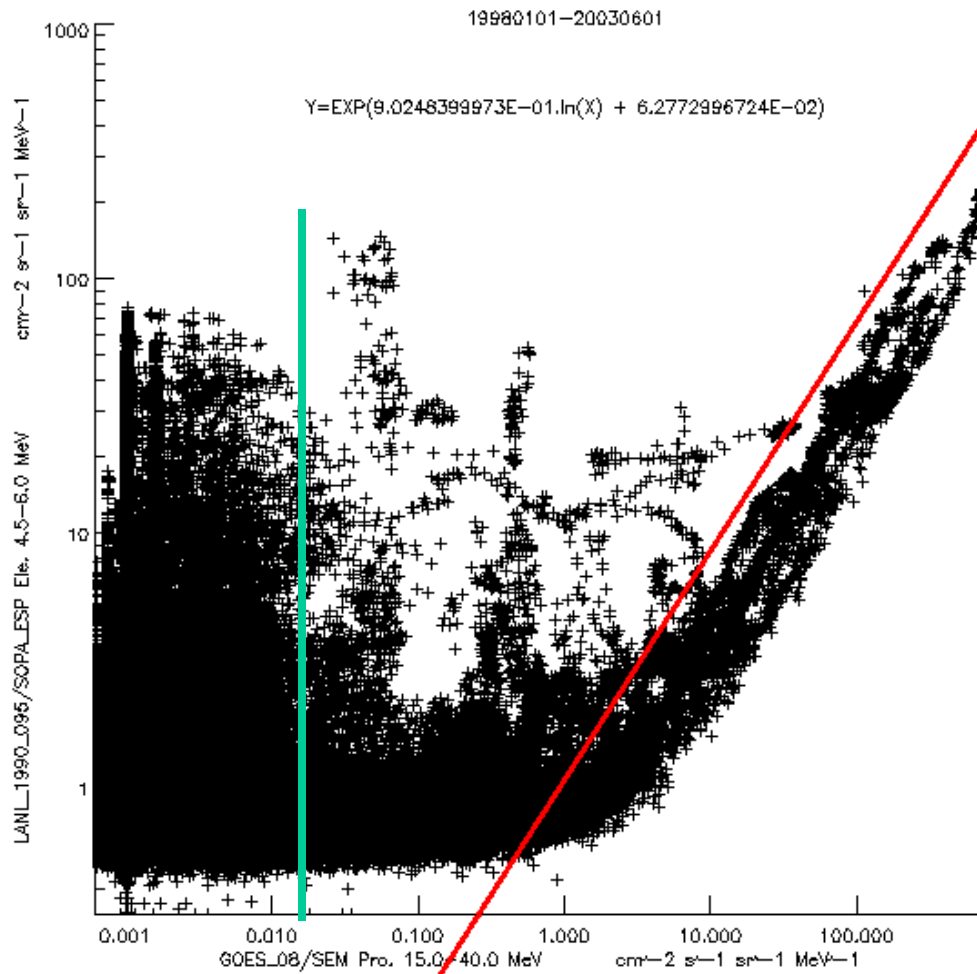
Figure 3 : Correlation plot between LANL-1990-095 Ele. 4.5-6. MeV and GOES-08 Pro. 15-44. MeV. Vertical green line indicates the threshold value above which GOES-08 detects SPEs. The red line indicates where the LANL data are contaminated significantly (above red line electrons dominate, below the red line protons dominate in the channel)

2- To evaluate possible contamination in the inner belt, only a flux map in a L* versus time plot can help. See Figure 2, bottom panel. Then a filter function of L* can be defined.

Now let us consider the case where there are proton measurements (in the energy range responsible for any background) on the same spacecraft. In this case, the analysis becomes easier: correlation plots can be made between the electron channels under consideration and proton channels. The best correlation is sought. If none is found, then there is no significant contamination in the electron channels..

In the case a correlation is found, data can be cleaned up as described above, where GOES data is replaced by the proton data measured on the same spacecraft.

IV.1.2 Contamination by relativistic electrons

In the case of electron channel, measurements can be contaminated by Bremsstrahlung photons. There is no easy way to get clear evidence of this kind of contamination except from Monte-Carlo simulation of the detector sensitivity to energetic electrons and/or by looking carefully at flux maps in a L* versus time plot. Such contamination is more likely to occur one or two days after a storm onset when electron spectra are harder in the outer belt.
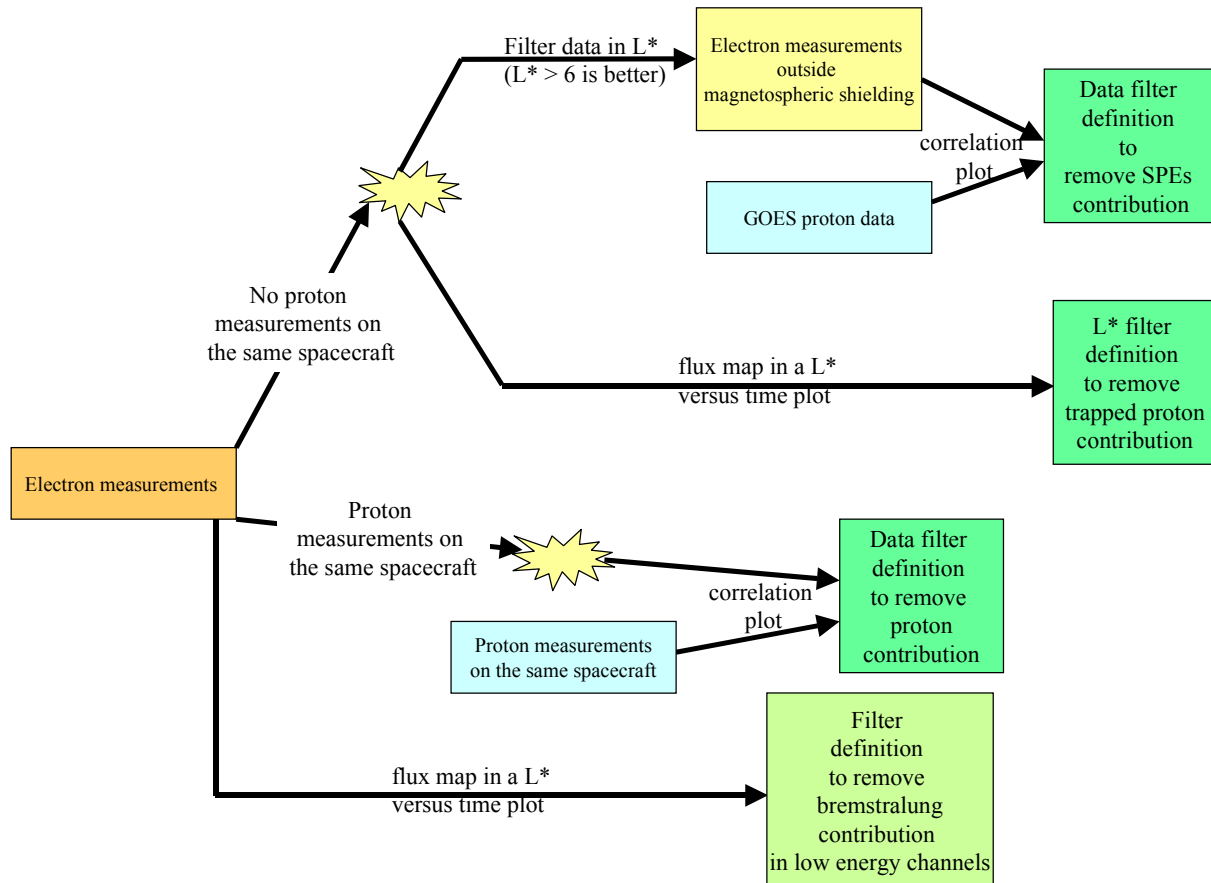
IV.1.3 Summary

Figure 4: Logic to define data filter to remove any contamination in trapped electron measurements.

IV.2 Proton data contamination

IV.2.1 Contamination by relativistic electron

Contamination in the proton channels frequently results from high energy electrons. This problem occurs preferentially in the outer electron belt. Clear evidence of such contamination can be seen on flux map in a L* versus time plot if no electron measurements are available on the same spacecraft, otherwise from correlation plots with various electron channels. An example is provided in Figure 5 where the proton channel 28.7-33.1 MeV on-board XMM spacecraft is contaminated by relativistic electrons during intense magnetic storms (inside the red oval). Since the events shown are above L=2.8 which is outside the proton trapping boundary for this energy, the measurements must be due to background. The same thing can

be seen on Figure 6 where the same proton channel is plotted versus electrons in the > 2.54 MeV channel, measured on-board the same spacecraft for regions above L=2. These correlations are used to define a filter to decontaminate the proton channels from the relativistic electron contribution.
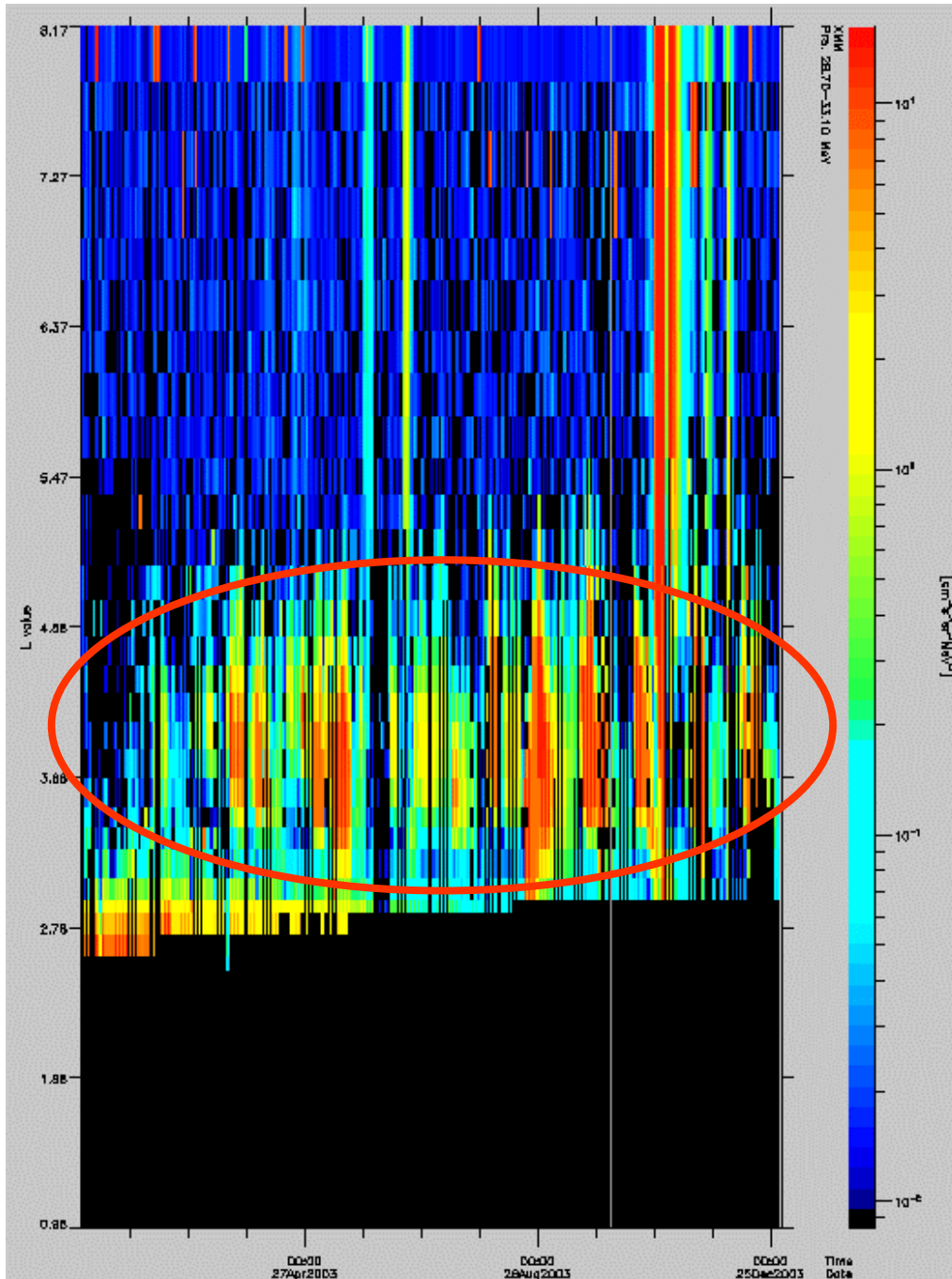

Figure 5: Example on proton contamination by electrons (inside red oval) on-board XMM spacecraft
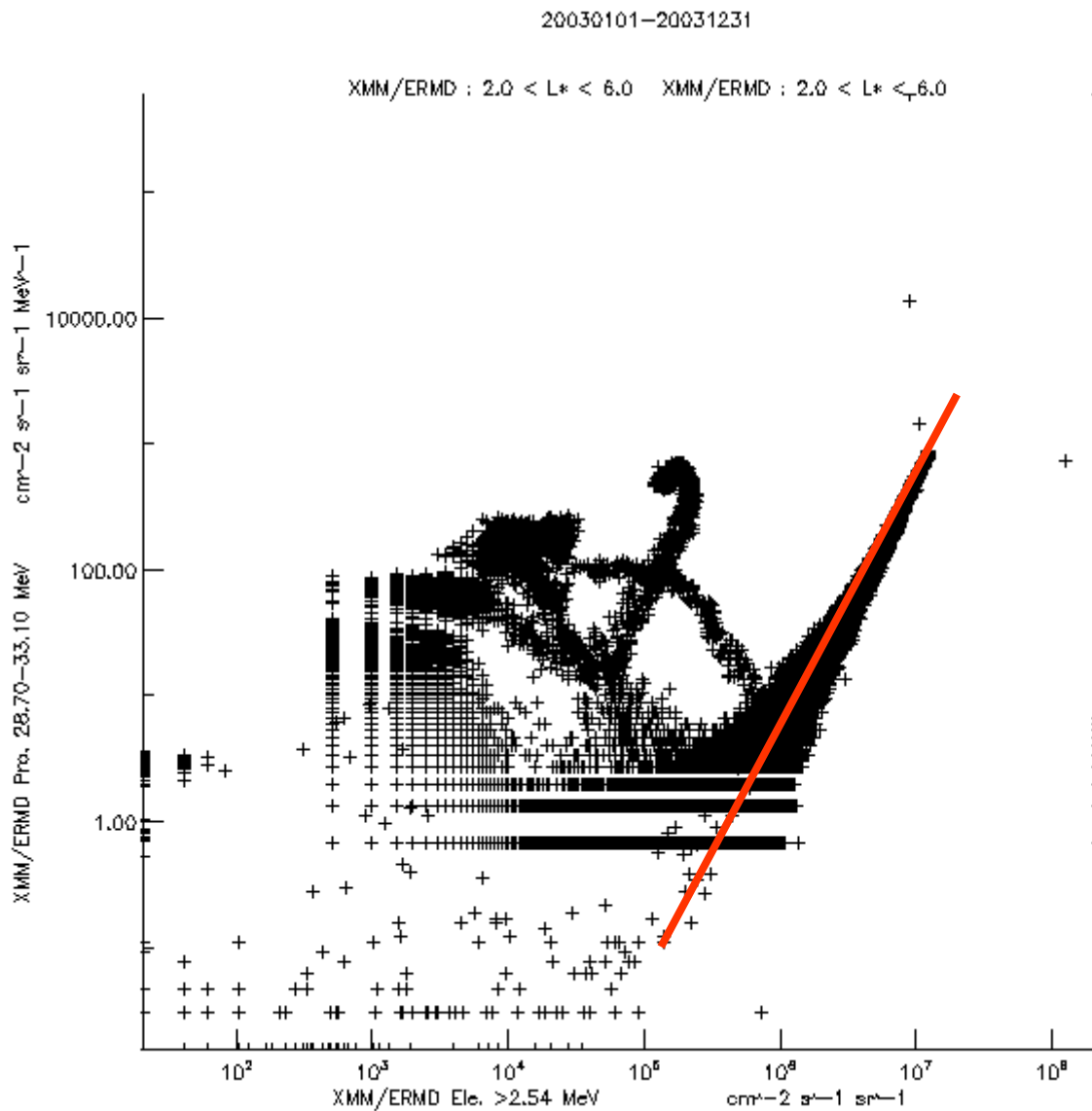
Figure 6: Correlation plot between a proton channel (28.7-33.1 MeV) and an electron channel (>2.54 MeV) on-board XMM. The red line shows when both are well correlated: electrons dominate protons.
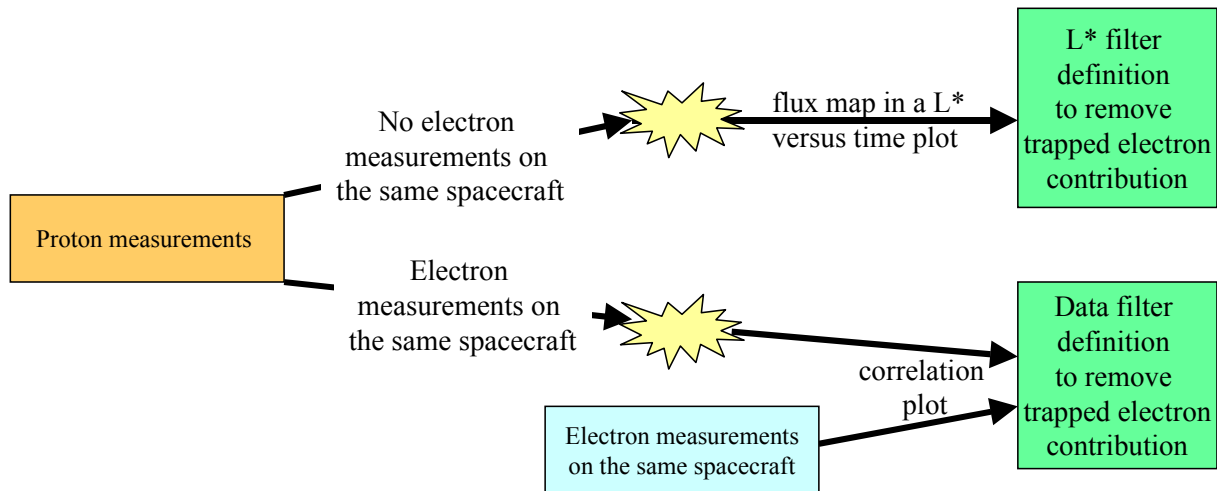
IV.2.2 Summary

Figure 7: Logic to define data filter to remove any contamination in trapped proton measurements

IV.3 Saturation

Count rate saturation occurs in some instruments leading to an artificial plateau in the observed count rate. These plateau levels are statistically observable, and it must be ensured that only data below saturation levels are used. Figure 8 shows the fraction of observations of a given flux level (of total observations) for one of the channels on the POLAR HISTe instrument across a range of L-values. The high plateau in flux observed in the L=4-5 region, in the center of the radiation belts, is a saturation effect for this instrument. Such saturation limits are normally only due to electronic processes and are normally stable in time. However, some instruments such as the POLAR HIST instrument are thought to have a variable dead time and thus a variable saturation limit, probably arising from a dependence of upon the nature of the background causing saturation.
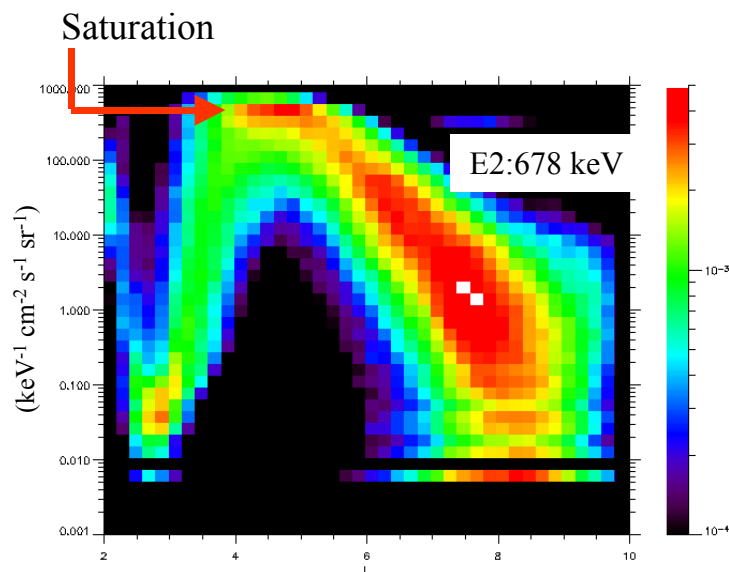

Figure 8: Fraction of observations of a given flux level (of total observations) for the 678 KeV electron channel of POLAR HISTe showing the saturation

Thus the saturation value for a given channel can be determined from careful scrutiny of the observations binned in flux and L*. After several refinements the threshold flux value above which the instrument saturates can be determined.

IV.4 Background

Background levels due to thermal noise or other contamination such as cosmic rays are present in all particle instruments. These levels can be detected by examining data during intervals when the spacecraft are outside the trapping region for energetic electrons. For example, this occurs over the polar cap on open field lines for LANL-GPS and during extreme magnetospheric compression events for the geosynchronous region. These background counts or fluxes must be detected and tracked over time and these counts or fluxes must be subtracted before any use of the data.

Figure 9 shows the background levels detected for LANL-GPS NS18 in the first electron channel. The LANL-GPS orbit routinely leaves the trapping region for energetic electrons due to its inclined orbit, sampling field lines that are no longer closed at large L*-values. During those times only the background and noise counts are observed. The background can be seen as the low count plateau at the low cumulative probability values (GPS spends approximately 30% of its time in open field line regions).
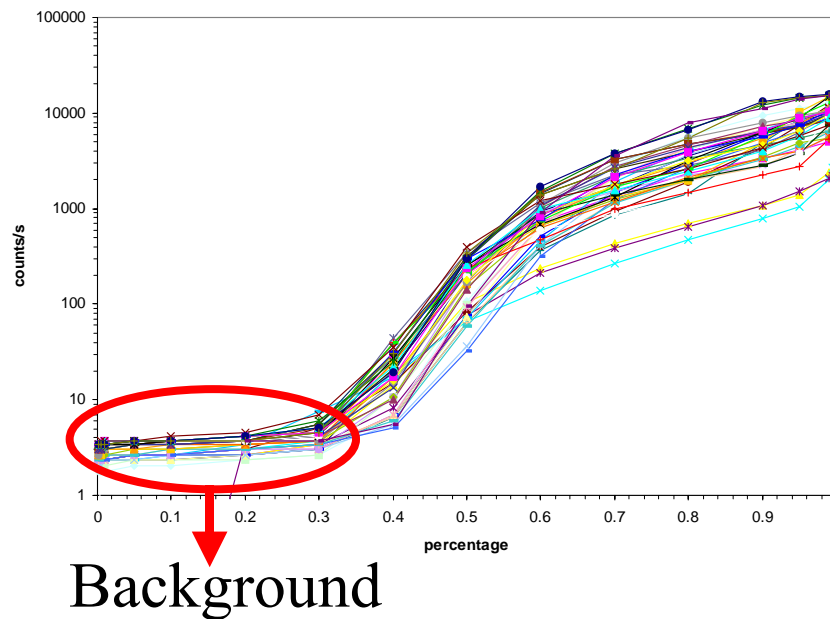

Figure 9: The cumulative probability of observed counts for GPS ns18, for a number of passes through the outer radiation belt. Each colored curve shows for one month the fraction of observations made at count levels below the maximum count observed during that month.

This observed background level may also depend on time. As silicon detectors or micro-channel plates age on-orbit , the background counting rates may increase. The galactic cosmic ray background has a solar cycle variation. Figure 10 shows the variation of the background levels for GPS NS18 from 1990 to the middle of 1994.
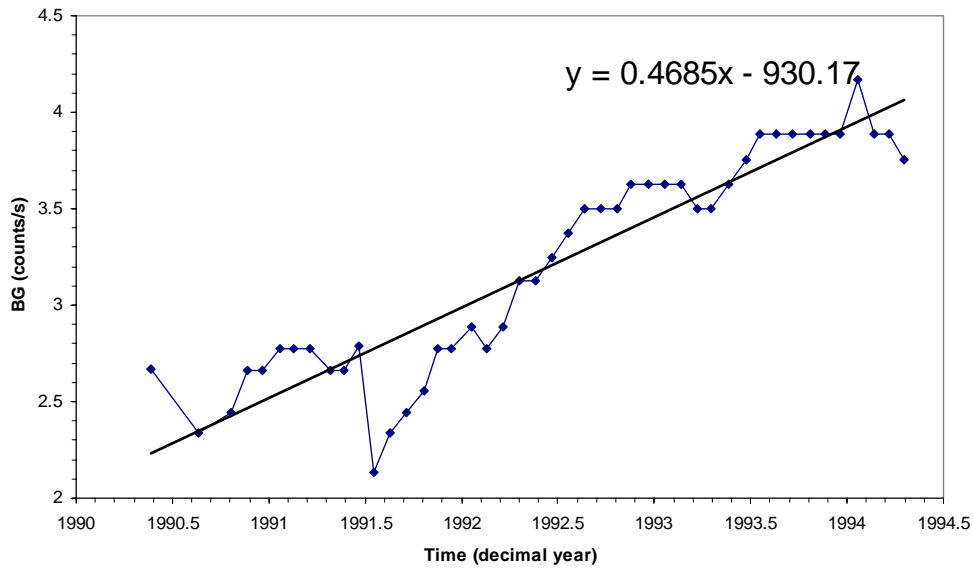
Figure 10: Variation of GPS ns18 background count levels over time (one point per month).

The background levels due to the GCR must be subtracted from the data. In most cases this is a small correction, because the count rates due to magnetospheric particles are generally much higher than the background levels due to the GCR. This correction does become important where the count rates are low. Because when count rates are very low the count rate itself is subject to instrument discretisation, so the background value can oscillate from one time to the next. So another safety factor must be used to exclude any data that is within a factor of three of the average background levels.

Thus , a monthly background value must be defined as the low count (or flux) plateau at the low cumulative probability values. Then for safety, three times the background level must be subtracted from the data and any resulting negative values need to be considered as "bad data".

IV.5 Signal to noise ratio.

Depending on the geometric factor of the instrument, for some energy channel the signal to noise ratio can be very low especially during quiet time or close to the edge of the radiation belts. In this case the discretisation of the instrument can be clearly seen. Such an example is shown in Figure 11 where on the left hand side, the fraction of observations binned in flux and L* is plotted. At low flux values each individual horizontal line shows the discrete value available on the instrument. Of course this adds errors on the flux value itself as shown on the right hand side of Figure 11 where MDS-1 data (for L*>5) are plotted versus GOES data (uncertainties in MDS-1 measurements at low flux values induce a scattered plot when compared to GOES). Times when such uncertainties are recorded must be removed.
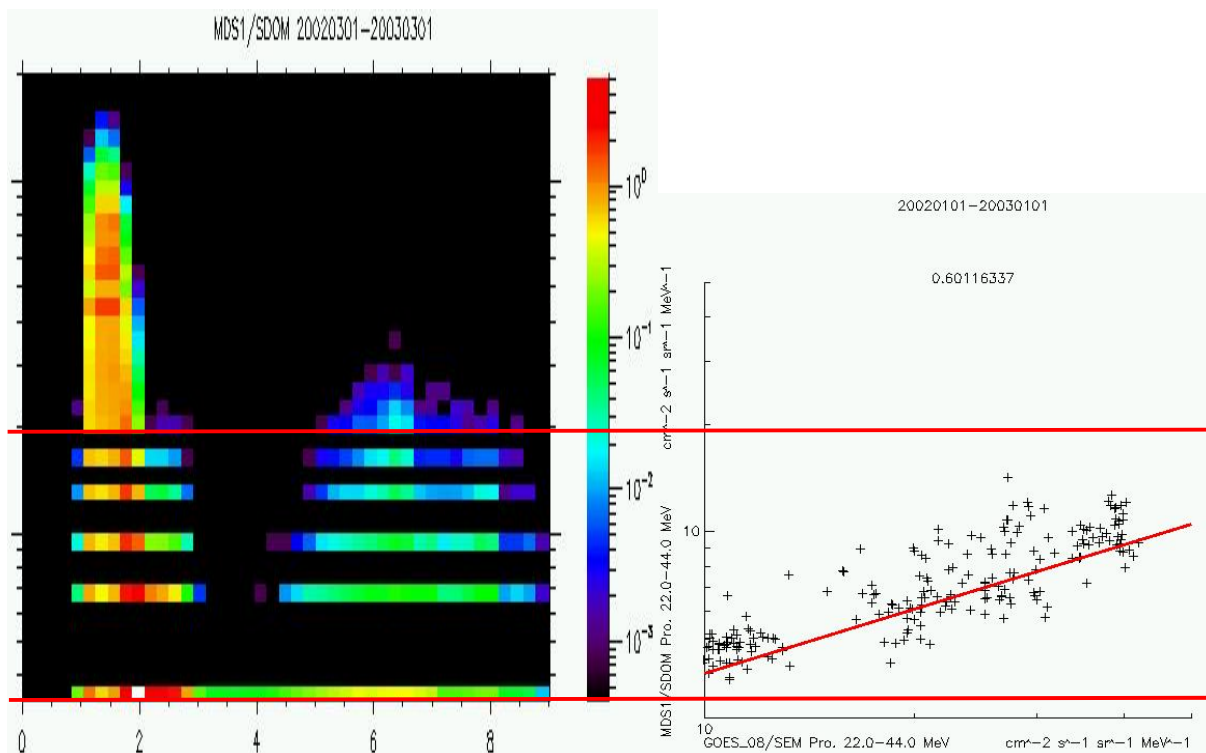
Figure 11: (left) fraction of observations from MDS-1 (22-44 MeV proton) binned in flux and L* and (right) correlation between MDS-1 (L*> 5) and GOES data

IV.6 Spacecraft charging bias.

For low energy measurements (i.e. cold plasma measurements) it is well known that the proton and electron energy seen by the plasma instrument can be shifted because of the absolute potential of the spacecraft. In the typical case, protons are accelerated whereas electrons are decelerated because the spacecraft acquires a negative potential with respect to the ambient plasma. To take this effect into account the spacecraft potential must be known. This can be done by looking at the proton spectrum where the energy of the peak flux (protons are accelerated to the same energy) gives the value of the spacecraft absolute voltage. Then measurements done at electron and proton energy lower than the spacecraft absolute voltage are not correct and must be removed, and the remaining spectrum needs to be shifted by the spacecraft potential.

IV.7 Other problems

By plotting the data in many different ways, e.g. flux versus latitude-longitude or time line plots, …, some additional problem in the data may be found. It could be bad spacecraft location, glitches, spikes … An example is given in Figure 12 where some spikes on GOES data can be found. In this case an appropriate filter/editing must be defined.
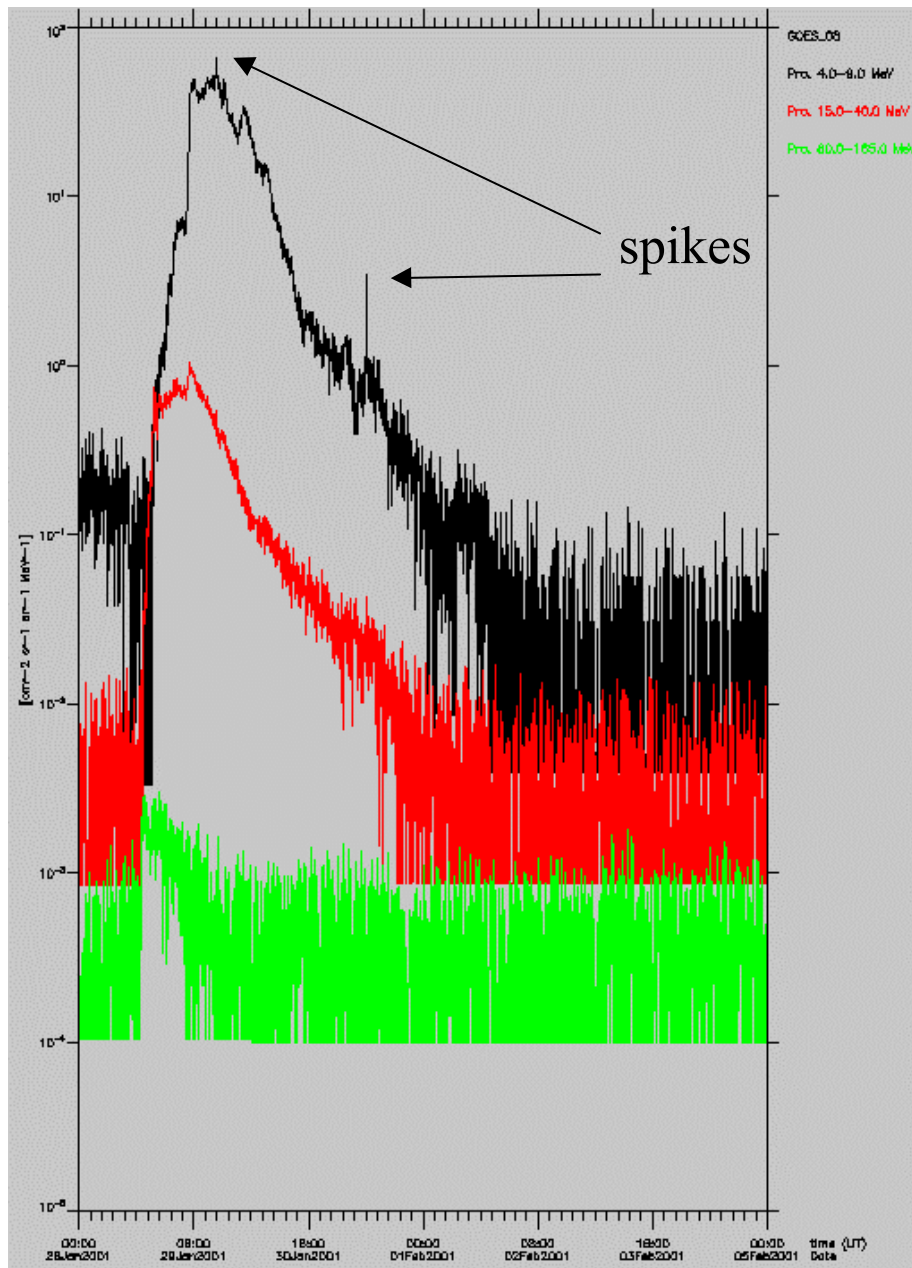
Figure 12: GOES proton data showing spikes in the instrument response

V Obtaining coherent data

V.1 Inter-calibration based on trapped particle dynamics

Given the limitations of each individual instrument's calibration, further on-orbit calibrations have to be resorted using the actual data collected. For this the best available instrument calibrations, some simple assumptions, a great deal of knowledge of the magnetospheric environment and dynamics, and the basic physics of the transport processes for energetic electrons can be used. Criteria that tell us when we can compare data between instruments on

two spacecraft, and how to propagate these comparisons forward and backward in time have to be established. A "gold standard" as a basic reference for on-orbit comparisons has to be defined. Inter-calibration will then consist of a simple scaling of all other instrument's spectra to a "gold standard". Inter-calibration is done using only omnidirectional fluxes, since not all instruments yield pitch-angle sorted fluxes and because use of such detailed data for this purpose would be a prohibitively huge task. In case of unidirectional measurements, they are integrated in pitch-angle before applying the following rules.

The basic assumption here is that each instrument measures a representation of a spectrum independent of count rate or spectral hardness, and that the simple scaling addresses uncertainties in each instrument's effective geometric factor and efficiency. It is known a-priori that some of these assumptions are violated at times, and that they ultimately need to be addressed in each instruments' fundamental response function. However, in the absence of such calibrations we have to start somewhere, and hope to achieve a set of inter-calibration factors that are at least valid most of the time. This is an on-going process - both to incorporate continuing new data sets and to incorporate updated higher fidelity instrument calibrations as they become available.

As mentioned before, the on-orbit calibration procedure relies on having a "gold-standard" - a reference instrument that is trusted to perform the best and cleanest measurements possible. In the case of electrons, the MEA instrument on CRRES is chosen for energies between 300keV and 1.6 MeV, since it was the last scientific instrument to fly in the equatorial region covering the inner magnetosphere from L=1.2 to 7.5. MEA was a magnetic spectrometer, measuring electrons in the range of 120 keV to 1.2 MeV. A magnetic spectrometer used magnetic deflection to bend incoming electrons onto a detector, which is an energy selective process. Pulse height analysis for the detectors provided a second energy discriminator, while a background detector that electrons could not normally reach provided a good determination of the penetrating background.

In case of protons, the SEM instrument on GOES-08 is chosen for energies between 10 and 100 MeV. GOES proton data are now well known throughout the world and this database is more or less considered as a standard. Corrected differential channels are then used. As those measurements concern non trapped protons (except P1) see next paragraph for how to start from there.

Next adjustment factors based on spacecraft conjunctions need to be found. A strict definition of a spacecraft conjunction would be based solely on the actual location of two spacecraft – defining a minimum distance between them. Such a definition would however yield a very small or even zero number of conjunctions for most spacecraft pairs. A more relaxed definition based on the geomagnetic coordinates discussed in the previous section, and on current knowledge of particle motion and magnetospheric activity can be used. The aim is to obtain a statistically meaningful set of conjunctions that enable the derivation of good adjustment factors between the two instruments under investigation.

Referring to Figure 13 the following list of conditions defining a "conjunction" are used:

1. $L^* < 6.$ and $\Delta L^* < 0.1$
2. $\Delta(B/B_{eq}) < 0.1$ and B/B_{eq} as close as possible to one
3. Magnetic Local Time (MLT) within 2 hours of 06 :00 and 18 :00
4. Magnetospheric activity quiet ($Kp < 2$) for two days before conjunction
5. $\Delta t < 3$ hours
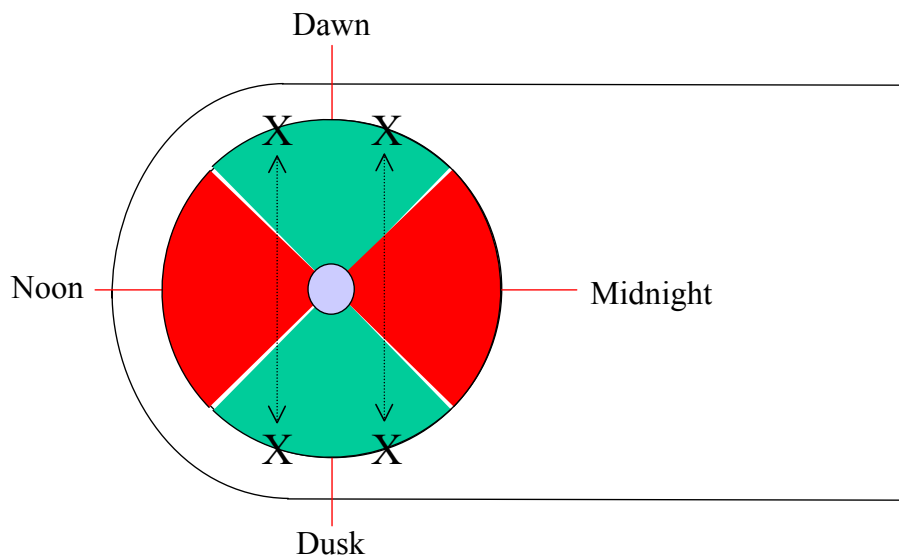6. Particle energy > 100 keV (particle must be trapped)

Figure 13: Schematic showing the green region of "allowed" conjunctions. Corresponding "X" indicate two possible conjunctions.

The first constraint is the most strict, requiring the measurements to be made very close to the same drift shell. The limit on $\Delta(B/B_{eq})$ restricts conjunction such that both instruments can sample the same particle distribution and $B/B_{eq} \sim 1$ restricts conjunction to the geomagnetic equator, ensuring that both instruments can sample the same full particle distribution (all particles bouncing along a field line go through the geomagnetic equator). The restriction in local time is due to the use of model magnetic fields in obtaining the required model coordinate L*, which performs best in these regions as this choice of location excludes compression events around noon and substorm-related dynamics around midnight. The low activity requirement allows one to relax the time constraint on conjunctions, and to exploit the noon-midnight symmetry of drift shells (it is possible to inter-calibrate instruments which are positioned symmetric relative to the noon-midnight plane). During low activity it is less likely to see loss or source events, and trapped particle fluxes are generally uniform in MLT around a drift shell. Furthermore, magnetic field models generally perform better during these times as well, yielding better estimates of L*. The use of the Olson-Pfitzer quiet model is more than enough.

Once a set of conjunctions has been found in this manner we find an adjustment factor for each energy channel that matches the target instrument's data to our gold-standard. We collect all these adjustment factors and find a statistical average factor across all conjunctions, ignoring factors outside of one standard deviation.

The procedure described here has been applied to LANL-GPS-CRRES, LANL-GEO-CRRES, LANL-GPS-POLAR, LANL-GEO-POLAR and LANL-GPS-LANL-GPS conjunctions, but not to GEO-GEO which never have conjunctions of this nature. For GEO-GEO a long-time average comparisons has been used, since many missions are available in statistically the same orbits (Figure 14).
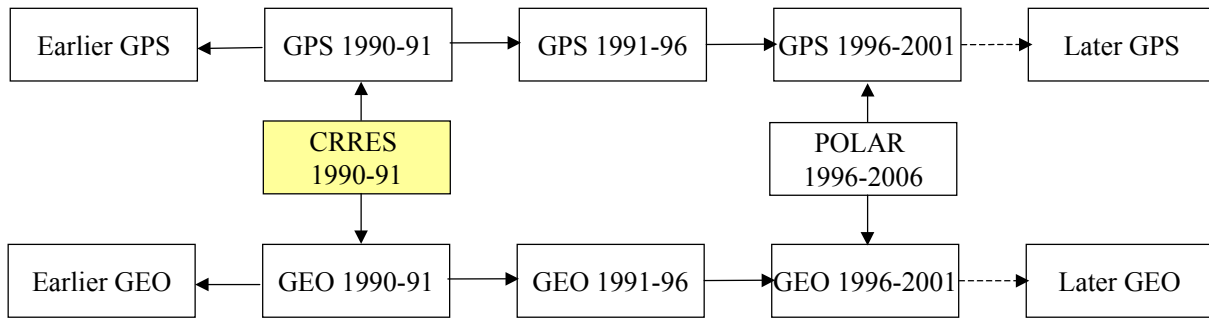
Figure 14: Example of mission time line for application of inter-calibration procedure in the case of electron measurements.

V.2 Inter-calibration based on SEP

To inter-calibrate high energy proton measurements (E>5 MeV) another alternative is available. It is possible to correlate proton measurements done by two different spacecraft when they are located outside of the geomagnetic shielding (L*>7 is fine except for GEO where L*>5.5 can be considered carefully – in this case the procedure is safe for E> 10 MeV). Under these conditions, during solar flares a good correlation should be obtained.

Starting from the existing calibrated channels of the "gold standard" (flux) the flux values at the "target" instrument channels can be evaluated by interpolation assuming a power law spectrum. This can accommodate both integral and differential "target" channels. These will then form the set of equivalent channels for comparison from which a set of adjustment factors will be found. The last step is to plot the data at the same time resolution when they exceed the background level (i.e. only during flares). Note that when GOES is used having 5 minutes time resolution works well.

Such an example is provided in Figure 15 where GOES data are interpolated such as to reconstruct the same channel as the one of SAC-C. SAC-C (715 km 98°) data are filtered such as only measurements done when L* is greater than 7 are kept. In a log-log plot the slope of the fit (in red on the Figure 15) which crosses the origin gives the inter-calibration coefficient.
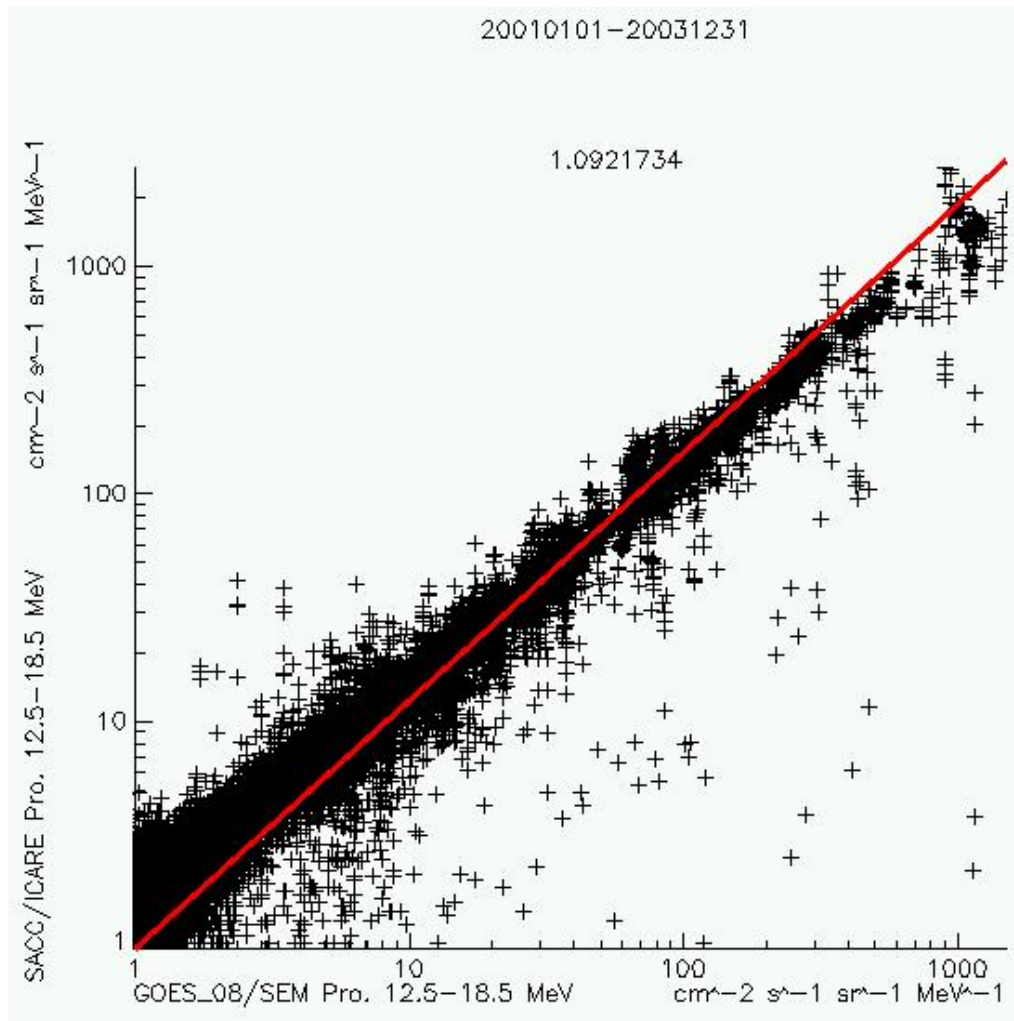
Figure 15: Correlation between SAC-C proton 12.5-18.5 MeV with GOES-08.
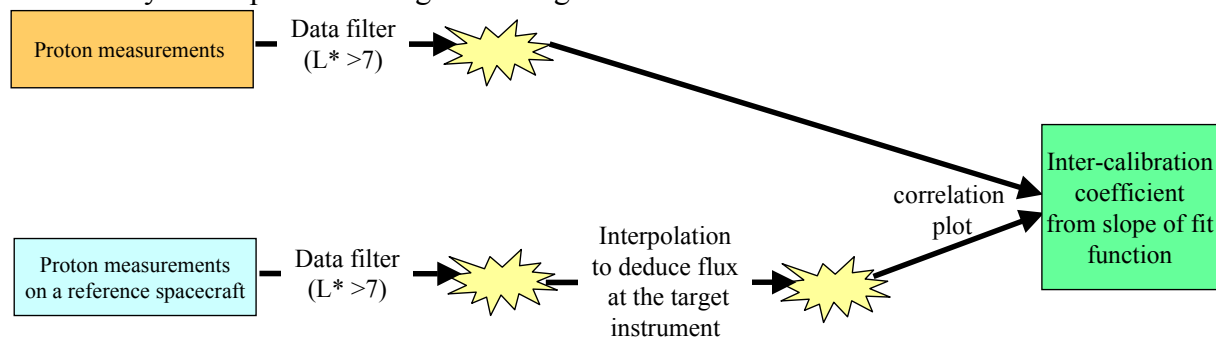
A summary of the procedure is given in Figure 16.

Figure 16: Logic to cross-calibrate proton measurements based on solar flares

V.3 Inter-calibration of cold plasma data

To date there are no clear techniques developed to inter-calibrate cold plasma data. Because of the low energy particle (E<50 keV) motion, the definition of a conjunction must consider

magnetic and electric fields. Most difficulties come from the introduction of electric field for which there are no good models in existence. In this context data must be considered as it.

VI Annex A1 : Trapped particle motion and their associated parameters.

A1.1 Trapped particle motion in a static dipole field.

In a static dipole magnetic field, particles with charge q are subject to the Lorentz force **F**:
$$\mathbf{F} = q \, (\mathbf{v} \times \mathbf{B}) \tag{A1}$$
where **v** is the particle velocity and **B** the local magnetic field vector. If the particles are not too energetic, their motion can be divided into three different elementary periodic motions (combined together).

The first one is the gyration around the field line. The radius R of the particle trajectory, called the Larmor radius, is related to the local magnetic field value B by ($R = p_{\perp}^2 \big/ qB$), p⊥ is the component of p perpendicular to the magnetic field vector. This motion is periodic with a frequency $\Omega = qB/m$ (m is the relativistic mass of the particle, the order of magnitude of the period in the Earth vicinity is a millisecond). In fact, during this circular motion particles are interacting with different magnetic field strength. Then if the gradients of the magnetic field are very strong, R cannot be assumed as a constant for very energetic particles and their motion is no more periodic. As this motion is in general periodic, an adiabatic invariant can be defined:
$$J_1 = p_{\perp}^2 \big/ 2qB \tag{A2}$$
which is related to the well known relativistic magnetic moment.

The second periodic motion is the bounce along the field line, with back and forth motion between two mirror points where the magnetic field value is $B=B_m$. Because the first adiabatic invariant is kept constant along the particle motion, the equatorial pitch angle α_{eq} (the angle between the magnetic field vector and the particle velocity **v**=**p**/m) can be defined such as $\sin^2\alpha_{eq} = B_{eq}/B_m$ where B_{eq} is the magnetic field strength at the magnetic equator. As this motion is also periodic, the corresponding adiabatic invariant can be defined:
$$J_2 = \frac{1}{2\pi} \oint p_{//} ds = \frac{1}{2\pi} \oint p\sqrt{1 - B/B_m}\,.ds \tag{A3}$$
The time period for the bounce motion is on the order of 1s.

The third periodic motion is a drift around the Earth. The particle drifts from one field line to the other, conserving J_1 and J_2 constant. Because this motion can be assumed to be periodic an adiabatic invariant can be defined:
$$J_3 = \iint B.dS = \oint A.dl \tag{A4}$$

where A is the potential vector of the magnetic field. The time period for the drift motion is tens of minutes.

Though the three motions are periodic, the resulting combined motion cannot be exactly periodic as the particle never comes back rigorously to its initial position (it is only the case if there is a resonance between the 3 periods: $\tau_d = m\tau_r = n\tau_g$ where m and n are integer). This combined motion is called quasi-periodic as the particle comes back as nearest as possible from its initial location after a large number of drift periods.

As a summary if a particle is trapped in the Earth magnetic field then three adiabatic invariants can be associated: J_1, J_2 and J_3.

Now, because we first assume here a static magnetic field we can deduce that the particle energy is kept constant all along its motion: equation A1 when scalarized by v leads to:
$$\mathbf{v}.\mathbf{F} = \mathbf{v}.d\mathbf{p}/dt = dE = 0 \qquad\qquad (A5)$$

Then because the energy is conserved we can deduce:
-   from J_1 = cste, then B_m = cste along the particle drift
-   from J_2 = cste, then $I = \oint \sqrt{1 - B/Bm}.ds$ = cste (I is the integral invariant)

From J_3, it is possible to define the Roederer L* parameter such as $J3 = BoR_e^2/L^*$, where R_e is the Earth radius and Bo the magnetic field dipole value at the earth surface at the equator.

To conclude, in a dipole field trapped particle motion is fully defined with the following parameters: Bm = cste, I = cste, L* = cste and E=cste. The first three parameters are all three directly related to the magnetic field and they define a surface (a drift shell) along which particles with different energies have their trajectory. It is only the duration to make a complete drift around the Earth which is directly related to the particle energy.

A1.2 Trapped particle motion in a static non dipole field.

Because the picture is one step further more complicated we have now to verify which hypothesis considered in the previous paragraph a no more realistic and in consequence which equations are no more valid.
In fact in this case all assumptions are kept valid and the equations are still correct. Nevertheless some characteristics of the trapped particle motion will be modified.

B_m = cste along the drift motion is still true. Nevertheless, if B is not symmetric with respect to the magnetic equator (which is usually no longer a plane), the two mirror points are no more symmetric. Moreover, it is possible that there are two minima of the magnetic field strength along the field line (i.e. two equators). In that case, four mirror points can be found rather than two (a particle with given J_1, J_2 and J_3 is then going to bounce between two mirror points or the others, depending on the initial phase it has on the bounce motion).

I = cste along the motion is still true.

Because the magnetic field is non-axisymetric two different particles with the same energy, located on the same field line but with different pitch angles (i.e. same B_{eq} but different B_m

and I) will not drift along the same drift shell. This effect is well known as the shell splitting. An example is given in Figure 17.

Tsyganenko89
Kp=0,
xyzGSE=[7.,0.,0.]
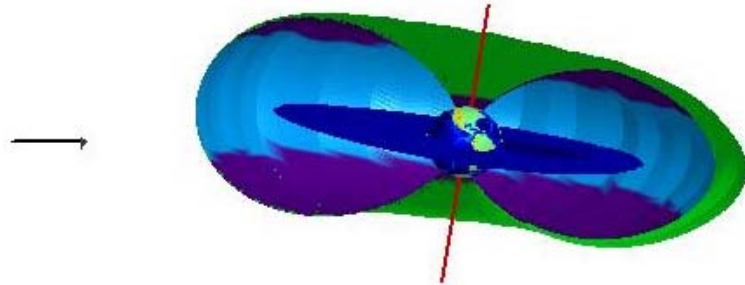PA=[70.°,4.°]
→L*=[6.315,6.628]

Figure 17 : Example of shell splitting. Two particles with different pitch angle (70° and 4°) are launched at the same position (xyzGSE=[7., 0., 0.] and follow a different drift shell, respectively L*=[6.315, 6.628].

A1.3 Trapped particle motion in a slowly dynamic non dipole field.

Let us complicate a little bit more the global picture, by considering a dynamic magnetic field. If the magnetic field slowly varies as compared to (all) the different periods of a trapped particle (gyration, bounce and drift) in a certain region of the space, then the three adiabatic invariants are really invariants (i.e. they are not violated): J_1 = cste, J_2 = cste, J_3 = cste.

From the Lorentz force point of view, an induced electric field must be considered:

$\mathbf{F} = q\,(\mathbf{E} + \mathbf{v} \times \mathbf{B})$ with $\mathbf{E} = -\delta\mathbf{A}/\delta t$,

This means that: $dE/dt = -q\,\mathbf{v}.\delta\mathbf{A}/\delta t$

In this situation it is no more possible to ensure that the energy is conserved ($\delta A/\delta t$ is modified during the particle gyration, bounce and drift motion). As a result B_m and I are no more constant. However, J_1, J_2 and J_3 are still constant, and

$$J_2 = \oint p\sqrt{1 - B/B_m}\,.ds = \oint \sqrt{2qB_m J_1}\sqrt{1 - B/B_m}\,.ds = \sqrt{2qJ_1}\oint\sqrt{B_m - B}\,.ds\,.$$

as J_1 is constant. It means that the integral:

$$K = \oint \sqrt{B_m - B}\,.ds \tag{A6}$$

not far from the Kaufmann parameter, is constant.